Dalton Transactions

Accepted Manuscript

Enhanced Upconversion Emission in ZrO_2-Al_2O_3 Composite Oxide

Yan Cong, Bin Dong*, Naisen Yu, Yangyang He, Ying Zhao, Yang Yang

School of Physics&Materials Engineering, Dalian Nationalities University, Dalian 116600, China

Aqueous solutions of zirconium oxychloride and aluminum nitrate were coprecipitated and crystallized to form a ZrO_2-Al_2O_3 solid solution. The upconversion (UC) emission from different Er^{3+}-doped samples was studied. Enhancement of the green UC emission by as much as 22 times was achieved by co-doping with Yb^{3+} and Mo^{6+} ions due to an energy transfer at a higher excited-state energy, which partly avoided the non-radiative decay processes at the lower energy levels of Er^{3+}. The UC emission of the ZrO_2-Al_2O_3 composite system series doped with different agents were both enhanced. Excess oxygen vacancies are generated by forming ZrO_2-Al_2O_3 solid solutions, which have an energy level close to the $^4F_{7/2}$ level of the Er^{3+} ions. The defect state promoted the energy trasfer process resulting in an eight-fold increased green UC emission in ZrO_2-Al_2O_3 solid solutions. The solid solutions has a superior color chromaticity of x=0.25 and y=0.71 due to the evident enhancement in the green to red emission ratio in the $8ZrO_2$-$2Al_2O_3$ sample.

* Correspondence author. Tel:+86-411-87924857; fax: +86-411-87556959.

E-mail: congyan@dlnu.edu.cn; dong@dlnu.edu.cn

1. Introduction

Upconversion (UC) luminescent materials with anti-stokes optical properties have garnered considerable attention because of their broad potential applications, including color display, solid-state lasers, sensor technology, solar cells and biological labeling.[1-5] Several rare-earth (RE) ions have been reported for their efficient UC luminescence. Among them, Er^{3+} ion which can efficiently emit photons in the green, red and near-infrared (NIR) regions is the most frequently used activator. Very often, Yb^{3+} is used as a sensitizer. Actually, as Yb^{3+} has a much larger absorption cross section than Er^{3+} near 980 nm, the NIR photon energy is efficiently transferred from Yb^{3+} to Er^{3+} resulting in an efficient energy transfer (ET).[3,4] Lately, much attention has been focused on the transition metal (TM) as sensitizer for RE ions. The intra-configurational d-d transitions in the TM resulting in low electron-phonon coupling and low multiphonon relaxation rate make the TM a potential sensitizer in UC luminescent materials.[5-7] In our study on the Er-Yb-Mo and Tm-Yb-Mo systems in oxidic matrix materials, we observed the intense UC luminescence in both.[5,8] Moreover, the luminescence efficiency also depends on the performance of the host material. To obtain a higher UC efficiency, the host should have low lattice phonon energy which can greatly reduce the nonradiative decay rate of multiphonon relaxations. Fluorides are efficient hosts for the UC luminescence of RE ions due to their appropriate energy phonons which produce strong UC emission. Compared with fluorides, oxides have high chemical durability, thermal stability and mechanical strength.[5,9,10] However their corresponding high phonon energies failed to suppress the nonradiative loss, resulting in weak UC emissions, which greatly hampers their applicability. To solve these problems above, the designing of new oxides materials capable of converting low phonon energy has been carried out.

ZrO_2-Al_2O_3 a composite oxide which can improve the current properties and create many new functions has attracted our attention. In the last two decades, ZrO_2 has been recognized as a new oxide host due to its low phonon energy (470 cm^{-1}), high chemical stability and broad optical transparence from visible to NIR wavelength.[10-12] Alumina is another important variety of oxide host for UC luminescence.[13,14] A ZrO_2-Al_2O_3 solid solution, formed by mixing Al_2O_3 and ZrO_2, is widely used as a potential catalyst, oxygen sensor, and hard ceramic material,[15,16] and most of the research has been focused on finding new synthesis methods to extend the Al_2O_3 in ZrO_2. A solution of this ZrO_2-Al_2O_3 composite oxide has received little attention as potential UC host material. Thus, it is very necessary to study the luminescent properties of this system in order to make the best use of it as a luminescent host.

Here, to improve the UC emissions in the oxide host, we prepared various ZrO_2-Al_2O_3 composites doped with different doping agents and studied the UC luminescent properties in detail. In the composite system, ZrO_2-Al_2O_3 composite samples which had been single-doped with Er^{3+} or tri-doped with Er-Yb-Mo both show a great enhancement of the UC luminescence. Characterization of the ZrO_2-Al_2O_3 composites series was performed by X-ray diffraction (XRD), Fourier transform infrared (FTIR) spectroscopy, UV-vis absorption spectroscopy and upconversion photoluminescence (UPL) emission spectroscopy. In addition, the enhancement mechanism of the UC emission in the ZrO_2-Al_2O_3 composites was investigated.

2. Experimental

2.1. Chemicals and materials.

$ZrOCl_2 \cdot 8H_2O$, $Al(NO_3)_3 \cdot 9H_2O$ and $(NH_4)_6Mo_7O_{24} \cdot 4H_2O$ were purchased from Sinopharm Chemical Reagent Co., Ltd. $Er(NO_3)_3 \cdot 5H_2O$ and $Yb(NO_3)_3 \cdot 5H_2O$ were purchased from Aldrich. All chemicals were of analytical grade reagents and were used directly without further purification.

2.2. Sample Preparation.

ZrO_2-Al_2O_3 solid solutions doped with different doping agents were prepared by the co-precipitation method. The synthesis procedure was as follows: 1 mmol $ZrOCl_2 \cdot 8H_2O$ (0.3223g) was dissolved under vigorous stirring in an aqueous solution

(50 mL). $Al(NO_3)_3 \cdot 9H_2O$ was added into the above solution according to the molar ratios of ZrO_2/Al_2O_3=2:8, 4:6, 5:5, 6:4, and 8:2. $Er(NO_3)_3 \cdot 5H_2O$, $Yb(NO_3)_3 \cdot 5H_2O$, and $(NH_4)_6Mo_7O_{24} \cdot 4H_2O$ with corresponding mole ratios (for 1 mol% Er^{3+}, 10 mol% Yb^{3+} and 10 mol% Mo^{6+}) were added into the above solution as doping agents. The polyethylene glycol (PEG, molecular weight=20000, A.R.) was added as a dispersant (0.02g/mL). A solution of 0.5 mol/L $NH_3 \cdot H_2O$ was slowly added into the solution as a precipitating aid agent until the pH was 7~8. The precipitate was suction-filtered, washed 4 or 5 times with de-ionized water, and dried at 100 °C to obtain a white powder. Finally, the as-prepared powder samples were annealed at 1100 °C for 3 h to produce the final samples. We denote the series of ZrO_2-Al_2O_3 samples as follows: $0.2ZrO_2$-$0.8Al_2O_3$ (**2Z-8A**), $0.4ZrO_2$-$0.6Al_2O_3$ (**4Z-6A**), $0.5ZrO_2$-$0.5Al_2O_3$ (**5Z-5A**), $0.6ZrO_2$-$0.4Al_2O_3$ (**6Z-4A**), and $0.8ZrO_2$-$0.2Al_2O_3$ (**8Z-2A**). In addition, the pure ZrO_2 doped with different doping agents were prepared by the same procedure above for comparison.

2.3. Characterization.

The structural characterization was performed by X-ray diffraction (XRD; Rigaku D/max-IIB) spectra with Cu Kα radiation (λ=0.15405 nm). The FTIR absorption spectra were measured by a Nicolet Avatar 370 FTIR spectrometer (Thermo Fisher Scientific, Waltham, MA, USA). UV-vis diffuse reflectance spectra were collected on a Lambda 750 UV/Vis/NIR spectrophotometer (Perkin Elmer, Waltham, MA, USA). UCL emission spectra were obtained on a Hitachi F-4600 fluorescence spectrometer, with an external 980 nm diode laser with a maximum power of 1 W and a focused area of 0.25 mm^2 as the excitation source, in place of the xenon lamp in the spectrometer. The spectrometer operated with excitation slit at 0 nm, and emission slit at 2.5 and 5 nm, respectively. The element analysis was performed on an inductively coupled plasma mass spectrometer (Optima 2000 DV, Perkin Elmer).

3. Results and Discussion

The XRD patterns of the ZrO_2 doped with Er, Er-Yb, or Er-Yb-Mo sintered at 1100 °C are displayed in Fig. 1(1). ZrO_2 has three crystallographic phases, namely the monoclinic (m), tetragonal (t), and cubic (c) phases. Bulk m-zirconia changes to t- and c-ZrO_2 at 1170 and 2370 °C, respectively. When doped with 1 mol% Er^{3+} ,the sample exhibits a monoclinic form with less amount of tetragonal form from the $(0,1,1)_t$ and $(1,1,2)_t$ reflections peaks at 30.2° and 50.2°, respectively. However, the tetragonal phase was stabilized when the sample was doped with 10 mol% Yb^{3+}. Oxygen ion vacancies can be generated via doping trivalent cations within the ZrO_2 lattice. Actually, the stability of the tetragonal phase in ZrO_2 has been attributed to the presence of oxygen vacancies produced by doping an appropriate amount of oversized trivalent cations. [17] When co-doped with 10 mol% Yb^{3+} and 10 mol% Mo^{6+}, the dominant crystalline structure turned to be a strong tetragonal phase containing traces of the monoclinic phase.

The XRD patterns of the Er-Yb-Mo tri-doped ZrO_2-Al_2O_3 solid solutions are summarized in Fig.1(2). The mixture of Al_2O_3 in ZrO_2 forms a solid solution of composition $Zr_{1-x}Al_xO_{2-x/2}$. During this phase transformation, the Al_2O_3 incorporates into the ZrO_2 lattice according to the following reaction equation:

$$Al_2O_3 \xrightarrow{ZrO_2} 2Al'_{Zr} + V_O^{\bullet\bullet} + 3O_O^X \qquad (1)$$

Nonequivalent substitution of Al_2O_3 for ZrO_2 produced Al'_{Zr} neagtiv defects and oxygen vacancies $V_O^{\bullet\bullet}$ and O_O^X. However, Al^{3+} (0.57Å) is apparently too small to substitute extensively for Zr^{4+} (0.79Å), resulting in a rather limited equilibrium solubility. The sample **8Z-2A** shows a dominant tetragonal ZrO_2 form contain traces of α-Al_2O_3. The α-Al_2O_3 reflection peaks in other samples (samples **6Z-4A** to **2Z-8A**) increased gradually. In addition, the ZrO_2-rich portion of the ZrO_2-Al_2O_3 system is a t-(Zr,Al)O_2 solid solution.[18] Actually, in the ZrO_2-Al_2O_3 system all the diffraction peaks corresponding to tetragonal ZrO_2 appear but display a systematic redshift. A close inspection of the XRD peak at 30.2° (0,1,1) in Fig. 1(2b) reveals that when the content of Al_2O_3 reached to 20 mol% in sample **8Z-2A**, the diffraction peak redshift was obvious, and no gradual shift in diffraction peaks occurred upon increasing the Al_2O_3 content. Accordingly, the redshift provides evidence of Al_2O_3 incorporation into the ZrO_2 lattice, and that no additional shift occured with the increase of the Al_2O_3 content, which is further evidence that the solid solution limit is about 20 mol% Al_2O_3, at which point no more Al_2O_3 could be incorporated into the ZrO_2 lattice.

Fig. 2 shows the UC emission spectra of pure ZrO_2 host with different doping agents upon laser excitation at the wavelength of 980 nm (1W/mm^2). By choosing suitable concentrations for the sensitizer and emitter molecules, an intense green UC emission was obtained with 1 mol% Er^{3+}, 10 mol% Yb^{3+}, 10 mol% Mo^{6+} tri-doped ZrO_2. The ZrO_2 single-doped with 1 mol% Er^{3+} radiated a green band at 550 nm ($^4S_{3/2}$-$^4I_{15/2}$ transitions), while a strong red band at 654/678 nm ($^4F_{9/2}$-$^4I_{15/2}$ transitions) was obtained after further doping 10 mol% Yb^{3+}. The strong red UC emission with the quenching of the green emission is due to the sensitization of Yb^{3+} to Er^{3+} which is well known and has been previously described.[3,4] ZrO_2 tri-doped with Er-Yb-Mo exhibits a great luminescence enhancement at 550 nm, corresponding to the $^4S_{3/2}$-$^4I_{15/2}$ transitions (22 times higher than the single-doped ZrO_2:Er^{3+}). Notably, the 525 nm green emission from the $^2H_{11/2}$-$^4I_{15/2}$ transitions, which are too weak to be observed in single-doped ZrO_2:Er^{3+}, markedly increased about 220 times in the Er-Yb-Mo tri-doped ZrO_2. Due to the extending emission region and the efficiently increasing emission intensity, a novel intense yellow-green UC emission was obtained in the Er-Yb-Mo tri-doped ZrO_2 phosphor. A similar enhancement was also observed in other Er-Yb-Mo co-doped oxidic matrix materials, such as Al_2O_3, TiO_2, Gd_2O_3, and CeO_2. We explain this intense UC emission as a special high excited state ET process, in which the ET occurs at a higher excited state energy ($|^2F_{7/2},^3T_2\rangle$ state of Yb^{3+}-MoO_4^{2-} dimer) thus avoiding the nonradiative decay processes that occurs at the lower energy levels of the Er^{3+} ions.[5,8,19]

Besides examining the effective sensitization of the Yb^{3+}-MoO_4^{2-}dimer, our study also focused on the evaluation of efficient host materials. Al_2O_3 mixed in a ZrO_2 matrix formed ZrO_2-Al_2O_3 solid solutions, and the UC luminescence properties of the ZrO_2-Al_2O_3 composite system series doped with different doping agents were investigated in detail. It is remarkable to see significant enhancement of the UC emission intensity in ZrO_2-Al_2O_3 solid solutions samples compared to the pristine oxide samples–ZrO_2 and Al_2O_3. It reveals that the composite oxide structure has a profound effect on the UC efficiency. The comparison of UC emission spectra for the series of ZrO_2-Al_2O_3 samples single-doped with 1 mol% Er^{3+} are shown in Fig. 3. The green emission is predominant one among all the Er^{3+} -doped composite samples. Additionally, the $^4S_{3/2}$-$^4I_{15/2}$ transition at 550 nm dominantly contributes to the green emission, as shown in Fig. 3. Actually, an increment in intensity is observed after introducing Al_2O_3 into ZrO_2 to produce the ZrO_2-Al_2O_3 composite oxide. The green emission at 550 nm increased in the ZrO_2-Al_2O_3 composite samples, and the strongest green emission is produced by sample **8Z-2A,** which exhibits about a 40–fold increment compared with the pure ZrO_2 sample. The significant increase of UC emission in sample **8Z-2A** may be due to the better miscibility of Er^{3+} in Al_2O_3-co-doped zirconia, which prevents the creation of large clusters and circumvents the concentration quenching process for the same concentration of Er^{3+}.[20,21]

The UC luminescence mechanism in Er^{3+} -doped systems, which has been well established in the literature,[3,4,20,21] is depicted in Fig. 4. First, the Er^{3+} ion is excited from the ground state $^4I_{15/2}$ to the excited state $^4I_{11/2}$. Subsequently, nonradiative relaxations of $^4I_{11/2}\rightarrow{}^4I_{13/2}$ also populate the $^4I_{13/2}$ level. Following first-level excitation, the excited atoms are excited from the $^4I_{11/2}$ to the $^4F_{7/2}$ levels or from the $^4I_{13/2}$ to the $^4F_{9/2}$ states. The populated $^4F_{7/2}$ may mostly nonradiatively relax to the $^2H_{11/2}$ and $^4S_{3/2}$ levels, which produce two green UC emissions. In addition, the red emission was obtained due to the $^4F_{9/2}\rightarrow{}^4I_{15/2}$ transitions. The mechanism of cooperative energy transfer process between two nearby Er^{3+} ions also contributes to the enhancement of green emission at the higher doping concentration. Two excited Er^{3+} at $^4I_{11/2}$ level interact with each other and one Er^{3+} is de-excited to $^4I_{15/2}$ level while the other is excite to $^4F_{7/2}$ level. The cooperative energy transfer becomes dominant in the sample with high Er^{3+} concentrations due to shortening the average distance between dopant ions and enhancing the interionic interaction.

The results of the element content analysis by ICP are listed in Table 1. The Er^{3+} ions content is 0.085 mol% for the **8Z-2A** sample, 0.024 mol% for the **6Z-4A** sample, 0.052 mol% for the **5Z-5A** sample, 0.044 mol% for the **4Z-6A** sample, and 0.026 mol% for the **2Z-8A** sample. This indicates that the $8ZrO_2$-$2Al_2O_3$ composite system benefits the efficient doping of Er^{3+}.

The absorption spectra of the series of ZrO_2-Al_2O_3 samples single-doped with 1 mol% Er^{3+} are shown in Fig. 5. The absorption band centered at 284 nm in the ZrO_2 sample corresponds to the host absorption. This band shows a blueshift in ZrO_2-Al_2O_3 composite samples, which is produced by an increase of the band gap caused by the stabilization of the tetragonal phase at 1100 °C. The main absorption peaks for Er^{3+} and the corresponding transitions are: 1524 nm ($^4I_{13/2}$), 962 nm ($^4I_{11/2}$), 652 nm ($^4F_{9/2}$), 525 nm ($^2H_{11/2}$), 490 ($^4F_{7/2}$), and 378 nm ($^4G_{11/2}$). The introduction of Al_2O_3 enhances the absorption properties of the Er^{3+} ions in these ZrO_2-Al_2O_3 composite samples. In particular, for the sample **8Z-2A** the absorption peak intensity exhibits a six-fold increment in the visible as well as the $^4I_{11/2}$ excited states near 980 nm compared with the sample without Al_2O_3. The enhancement of absorption by the $8ZrO_2$-$2Al_2O_3$ composite system can be attributed to higher doping concentration of Er^{3+} as mentioned above in the ICP results. The Er^{3+} ions in sample **8Z-2A**, which has the solid solution limitation of Al_2O_3, are localized at either the zirconium or aluminum lattice site that prevents aggregation. The bypassing of the nonradiative process ($^2H_{11/2}\rightarrow{}^4I_{9/2}$)/($^4I_{15/2}\rightarrow{}^4I_{13/2}$) due to cross relaxation, which leads to the decay of the $^4S_{3/2}$/$^2H_{11/2}$ levels, mostly radiatively to the $^4I_{15/2}$ level, and a remarkable 40-fold enhancement of the intensity.

The phonon energy of pure ZrO_2 is around 470 cm^{-1}, which makes it a good candidate to insert rare earth ions for UC photoluminescence applications. FTIR was performed to ascertain how the introduction of Al_2O_3 affects the phonon energy distribution in these hosts of solid solutions. For the pure ZrO_2 sample, the principal transmittance band is centered at 470 cm^{-1}, as shown in Fig. 6. This principal band shifts to longer wave numbers at 510 cm^{-1} in the ZrO_2-Al_2O_3 composite samples, which allows higher phonon energy to be produced. Additionally, the FTIR study reveals that the ZrO_2-Al_2O_3 composite has a lower hydroxyl group content. A broad band centered at 3435 cm^{-1} is due to the OH stretching vibrations of water, and the corresponding bending vibration is at 1640 cm^{-1}. Both of the peaks decrease in the ZrO_2-Al_2O_3 composite, and are mostly absent in the $8ZrO_2$-$2Al_2O_3$ composite sample. Surface hydroxyl groups can influence the nonradiative relaxation rate,[22] thus the hydroxyl content is another reason for the increase of the UC emission intensity observed in sample **8Z-2A.**

The ZrO_2-Al_2O_3 solid solutions also induced an increase of the UC emitted in the Er-Yb-Mo tri-doped samples. A high efficiency, as much as 22 times, in the green UC emission was achieved by tri-doping with Er^{3+}-Yb^{3+}-Mo^{6+} ions in pure ZrO_2 (Fig. 2). The high efficiency of the UC emission was further enhanced 8-fold in the $8ZrO_2$-$2Al_2O_3$ solid solutions. The UC emission spectra of the Er-Yb-Mo tri-doped series of the ZrO_2-Al_2O_3 composite system are shown in Fig. 7. Interestingly, the UC emission intensity in the ZrO_2-Al_2O_3 composite samples was enhanced compared with pure ZrO_2 and Al_2O_3 samples. The **8Z-2A** sample shows the strongest emission of all the samples studied and the relative emission intensity is about 7-and 8-fold increased compared with pure ZrO_2 and Al_2O_3 samples, respectively.

A simplified diagram illustrating the possible mechanism of UC emission and the energy transfer process is depicted in Fig. 8. Our previous work suggest that Mo substitutes for the tri-valent Yb^{3+} ions to form Yb^{3+}-MoO_4^{2-} dimmer. Accurate first-principles calculations show that configuration with Mo occupying Yb sites have a total energy lower than other configurations.[5] Firstly, the Yb^{3+}-MoO_4^{2-} dimer absorbs a 980 nm photon and is excited from the ground state $|^2F_{7/2}, {}^1A_1\rangle$ to the intermediate excited state $|^2F_{5/2}, {}^1A_1\rangle$ level (GSA). Next, the excited ion absorbs a second photon in an excited state absorption (ESA) process and is promoted to the relevant higher level of $|^2F_{7/2}, {}^1T_1\rangle$. The excited state of $|^2F_{7/2}, {}^1T_1\rangle$ is much higher in the Er-Yb-Mo system than in the Er-Yb-doped ZrO_2. The ET takes place at a higher excited state energy and partly avoids the nonradiative decay processes that occur at the lower energy levels of Er^{3+}, leading to the enhancement of the efficiency enhancement of the green UC emission in the Er-Yb-Mo tri-doped samples.[5,8,19] In the host of the ZrO_2-Al_2O_3 solid solutions, the oxygen ion vacancies ($V_O^{\bullet\bullet}$) can be generated as a result of charge balance by incorporating an appropriate amount of Al_2O_3, as shown in equation (1). The oxygen vacancy serves as the F center and greatly affects the luminescent properties in ZrO_2. The blue emission centered at 470-490 nm from ZrO_2 is attributed to the $V_O^{\bullet\bullet}$ defects.[23-25] Moreover, the $^4F_{7/2}$ level of Er^{3+} ions (490 nm) is very close to the defect state. When the above two-photon process occurs, the excited ions are easy to be captured by the $V_O^{\bullet\bullet}$ defects near the $|^2F_{7/2}, {}^1T_1>$ state, and then transfer to $^4F_{7/2}$ level of Er^{3+}. The presence of the $V_O^{\bullet\bullet}$ defects in the ZrO_2-Al_2O_3 system favors the promotion of the ET process, in which the Yb^{3+}-MoO_4^{2-} dimer sensitizes the Er^{3+} ions at the $|^2F_{7/2}, {}^1T_1>$ excited state, which nonradiatively relaxes to $^2H_{11/2}$ and $^4S_{3/2}$ levels and subsequently results in two strong green emissions. The red emission caused by populated $^4F_{9/2}$ level in the ZrO_2-Al_2O_3 system is one order of magnitude weaker than the green emission, as shown in Fig. 7, and provides further evidence of the high excited state energy transfer UC process.

The dependence of the green UC intensity (empty bars) and red UC intensity (shaded bars) on different ZrO_2-Al_2O_3 composite samples is depicted in Fig. 9. The intensity of the green emission relative to the intensity of the red emission is 8.12 and 3.06 for the sample **8Z-2A** and pure ZrO_2, respectively. A predominantly green emission was obtained, and as the ratio was 8:1, the emission was almost exclusively green in the sample **8Z-2A**. The evident enhancement in the green to red emission ratio in comparison with the ZrO_2 sample makes the ZrO_2-Al_2O_3 composite sample an efficient green UC phosphor with high color purity. The Commission Internationale del′ Eclairage (CIE) chromaticity coordinates of sample **8Z-2A,** calculated from the corresponding upconverted emission spectrum, is (0.25, 0.71), while the index of ZrO_2 is (0.32, 0.41). In addition, the corresponding hue of the samples are green and yellow-green, respectively, as indicated in the chromaticity diagram inset in Fig. 9. It is well known that the green and red UC intensities are proportional to the population of $^4I_{11/2}$ and $^4I_{13/2}$ levels, which are strongly governed by the nonradiative relaxation from the two levels. Thus, decreasing the nonradiative relaxation rate can increase the population ratio of the $^4I_{11/2}$ to $^4I_{13/2}$ levels, so as to enhance the green UC emission and suppress the red emission, simultaneously.

4. Conclusion

A series of ZrO_2-Al_2O_3 composites containing different zirconium compositions (20 to 100 mol%) were prepared by the co-precipitation method, and the optimum composition was determined to be $8ZrO_2$-$2Al_2O_3$. The visible green UC emission was significantly enhanced by doping with different dopant ions in the $8ZrO_2$-$2Al_2O_3$ composites. The enhancement of the green UC emission from the $^4S_{3/2}$-$^4I_{15/2}$ transition in Er^{3+} single-doped $8ZrO_2$-$2Al_2O_3$ is ascribed by reducing the nonradiative relaxation due to the better miscibility of Er^{3+}. The UC emissions were further increased by tri-doping Er^{3+}-Yb^{3+}-Mo^{6+} ions through a high ET process which occurred at higher excited state energy and avoided the nonradiative decay processes in the Er^{3+} ions. Furthermore, ZrO_2-Al_2O_3 phosphor exhibits high color saturation with the appropriate tuning of the concentration of the Al_2O_3 solid solution.

Acknowledgment

This work is supported by the National Natural Science Foundation of China (Grant Nos.11274057, 11474046, and 11474045), Program for New Century Excellent Talents in University (Grant No. NCET-13-0702), Science and Technology Project of Liaoning Province (Grant No. 2012222009), Fundamental Research Funds for the Central Universities (Grant No. DC201502080302, DC201502080203, and DC201502080406), Program for Liaoning Excellent Talents in University (LNET) (Grant No. LR2015016), and Science and Technique Foundation of Dalian (Grant No. 2014J11JH134, 2015J12JH201).

References

1. A.J. Silversmith, W. Lenth and R.M. Macfarlane, *Appl. Phys. Lett.* 1987, **51**, 1977.

2. A.R.S. Niedba, H. Feindt, K. Kordos, T. Vail, J. Burton, B. Bielska, S. Li, D. Milunic, P. Bourdelle and R. Vallejo, *Anal. Biochem.* 2001, **293**, 22.

3. A.S. Gercia, R. Serna, M.J. Castrc and C.N. Afonso, *Appl.Phys.Lett.* 2004, **84**, 2151.

4. J. Zhou, F. Moshary, B.M. Gross, M.F. Aark and G.A. Ahmed, *J. Appl. Phys.* 2004, **96**, 237.

5. B. Dong, B. Cao, Y. He, Z. Liu, Z. Li and Z. Feng, *Adv. Mater.* 2012, **24**, 1987.

6. D.R. Gamelin and H.U. Güdel, *Acc. Chem. Res.* 2000, **33**, 325.

7. O.S. Wenger and H.U. Güdel, *J. Phys. Chem. B* 2002, **106**, 10011.

8. B.S. Cao, Y.Y. He, Z.Q. Feng, Y.S. Li and B. Dong, *Sens.Actuators B* 2011, **159**, 8.

9. X. Bai, H.W. Song, G.H. Pan, Y.Q. Lei, T. Wang, X.G. Ren, S.Z. Lu, B. Dong, Q.L. Dai and L.B. Fan, *J.Phys.Chem.C* 2007,**111**,13611.

10. E.D. Rosa, P. Salas, H. Desirena, C. Angeles and R.A. Rodriguez, *Appl. Phys. Lett.* 2005, **87**, 241912.

11. A. Patra, P. Ghosh, P.S. Chowdhury, M.A.R.C. Alencar, W.L. B., N. Rakov and G.S. Maciel, *J. Phys. Chem. B* 2005,**109**,10142.

12. E.D. Rosa, P. Salas, H. Desirena, C. Angeles and R.A. Rodríguez, *Appl. Phys. Lett.* 2005,**87**,241912.

13. X.J. Wang, M.K. Lei, T. Yang and H. Wang, *Opt. Mater.* 2004, **26**, 247.

14. D. Liu and Y. Cong, *SCIENCE CHINA, Physics,Mechanics&Astronomy*, 2012, **55**, 1417.

15. B. Basu, J. Vleugels and O.M.D. Biest, *J. Alloys. Compds*. 2004, **372**, 278.

16. S.M. Chang and R. Doong, *Chem Mater*, 2007, **19**, 4804.

17. P. Li, I.-W. Chen and J.E. Penner-Hahn, *J. Am. Ceram. Soc.* 1994, **77**, 118.

18. M.L. Balmer, F.F. Lange and C.G. Levi, *J. Am. Ceram. Soc.* 1994, **77(8)**, 2069.

19. Y. Cong, D. Liu, N. Yu, Y. Xiao, Q. Yang and Y. Fu, *Mater. Chem. Phys*. 2014, **144**, 440.

20. A. Gedanken, R. Reisfeld, E. Sominski, O. Palchik, Yu. Koltypin, G. Panczer, M. Gaft and H. Minti, *J. Phys. Chem. B* 2000, **104**, 7057.

21. P. Amitava, S.F. Christopher, K. Rakesh and N.P. Paras, *J. Phys. Chem. B* 2002, **106**, 1909.

22. X. Wang, X. Kong, G. Shan, Y.I. Yu, Y. Sun, L. Feng, K. Chao, S. Lu and Y. Li, *J. Phys. Chem. B.* 2004, **108**, 18408.

23. Y. Cong, B. Li, B. Lei and W. Li, *J. Lumin.* 2007, **126**, 822.

24. T. Brankowa, V. Bekiari and P. Lianos, *Chem. Mater.* 2003, **15**, 1855.

25. M. Akiyama, C. Xu and K. Nonaka, *Appl.Phys.Lett.* 2002, **81**, 457.

Figure captions

Fig. 1 (1) XRD patterns of ZrO_2 doped separately with Er, Er-Yb, Er-Yb-Mo. (2)XRD patterns of the series of the Er-Yb-Mo: ZrO_2-Al_2O_3 solid solution samples (a), and partial enlarge detail of (0,1,1)t peak (b).

Fig. 2 UC emission spectra of the Er:ZrO_2, Er-Yb:ZrO_2, and Er-Yb-Mo:ZrO_2 samples (Emission slit=5 nm).

Fig. 3 UC emission spectra of the Er^{3+} doped series of the ZrO_2-Al_2O_3 composite system (Emission slit=5 nm).

Fig. 4 UC luminescence mechanism of Er^{3+}.

Fig. 5 Absorption spectra of the series of ZrO_2-Al_2O_3 solid solutions samples single-doped with 1 mol% Er^{3+}.

Fig. 6 FTIR spectra of the ZrO_2-Al_2O_3 solid solutions samples.

Fig. 7 UC emission spectra of 1 mol% Er^{3+}, 10 mol% Yb^{3+}, 10 mol% Mo^{6+} doped series of ZrO_2-Al_2O_3 composite system (Emission slit=2.5 nm).

Fig. 8 Schematic energy level diagram of the Er-Yb-Mo tri-doped ZrO_2-Al_2O_3 composite system.

Fig. 9 Dependence of the green UC intensity (empty bars) and the red UC intensity (shaded bars) on different ZrO_2-Al_2O_3 composite samples. Inset shows the CIE chromaticity diagram for the ZrO_2-Al_2O_3 composite and ZrO_2 samples.

TABLE 1: ICP Results of Different Samples

Y. Cong et al. Fig. 1

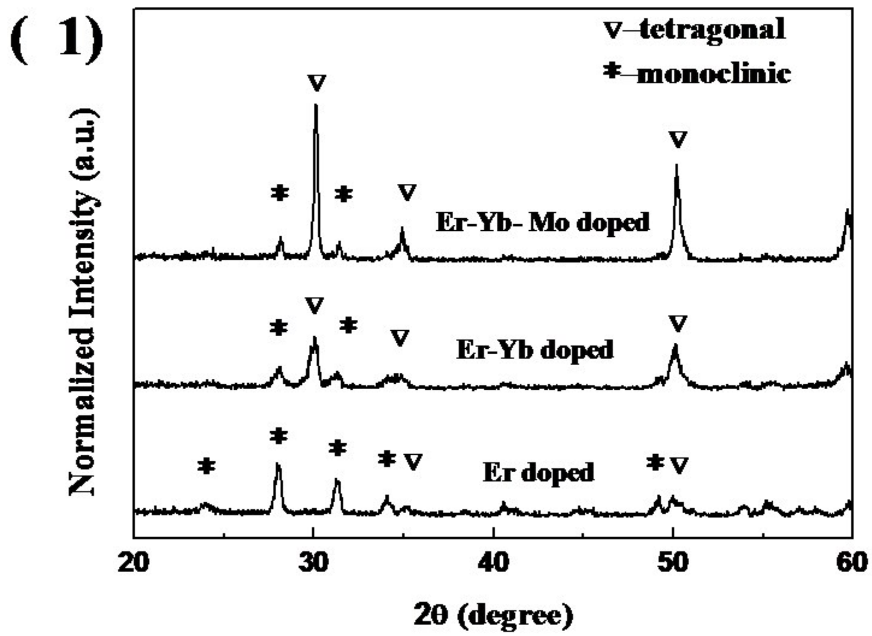

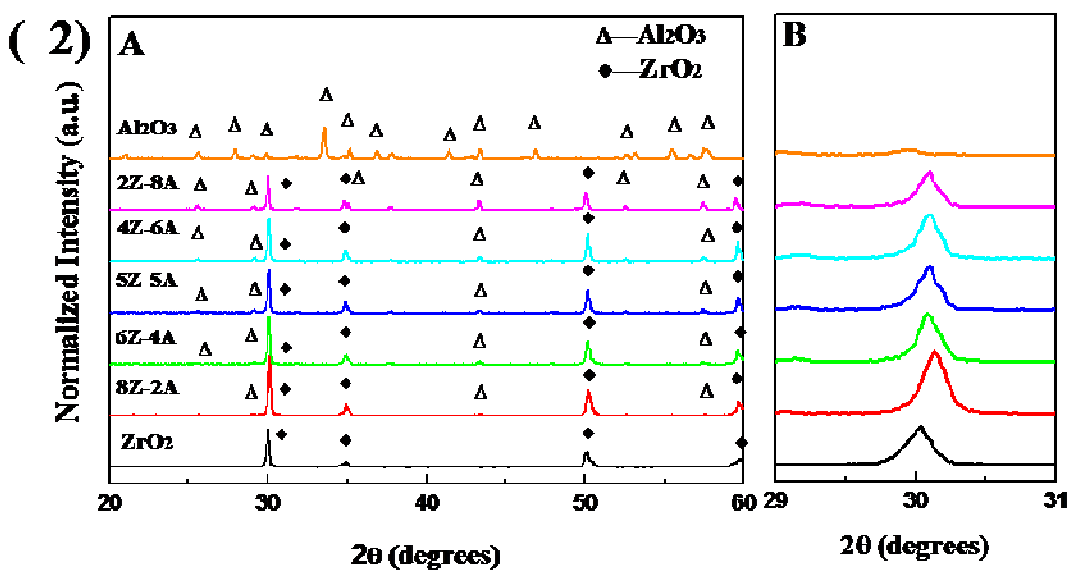

Y. Cong et al. Fig. 2

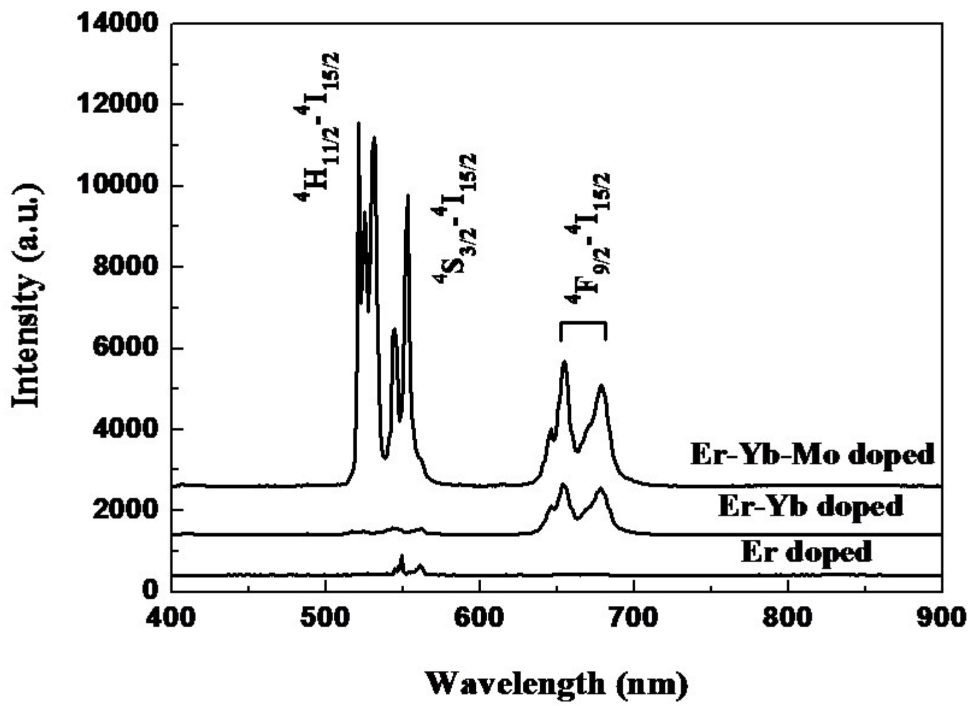

Y. Cong et al. Fig. 3

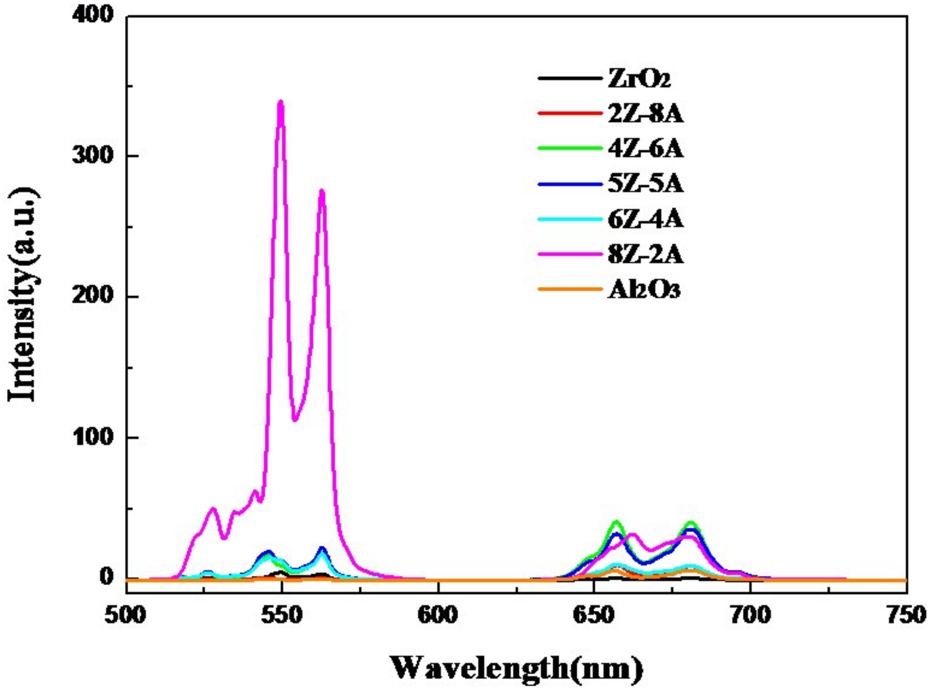

Y. Cong et al. Fig. 4

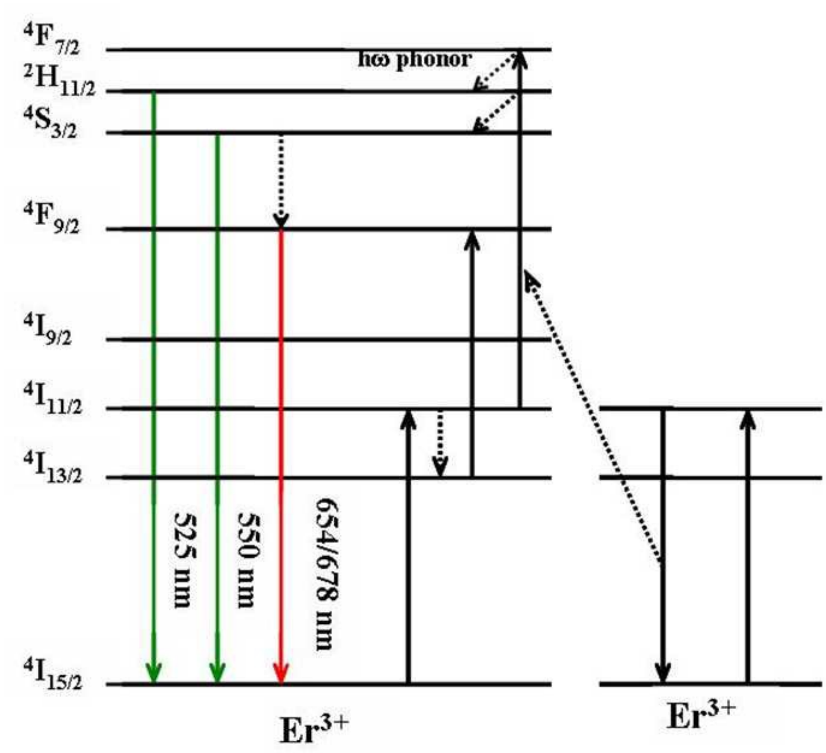

Y. Cong et al. Fig. 5

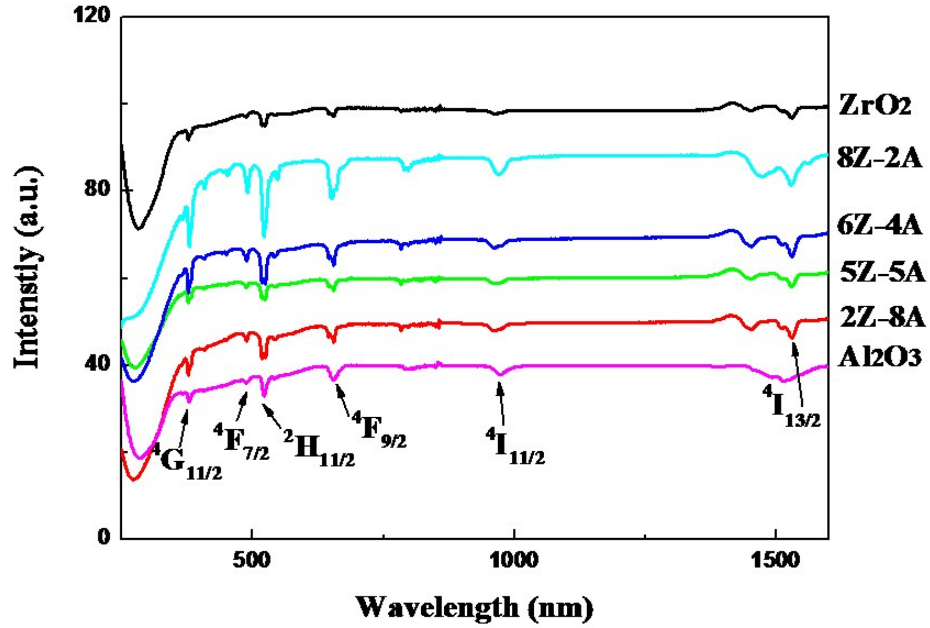

Y. Cong et al. Fig. 6

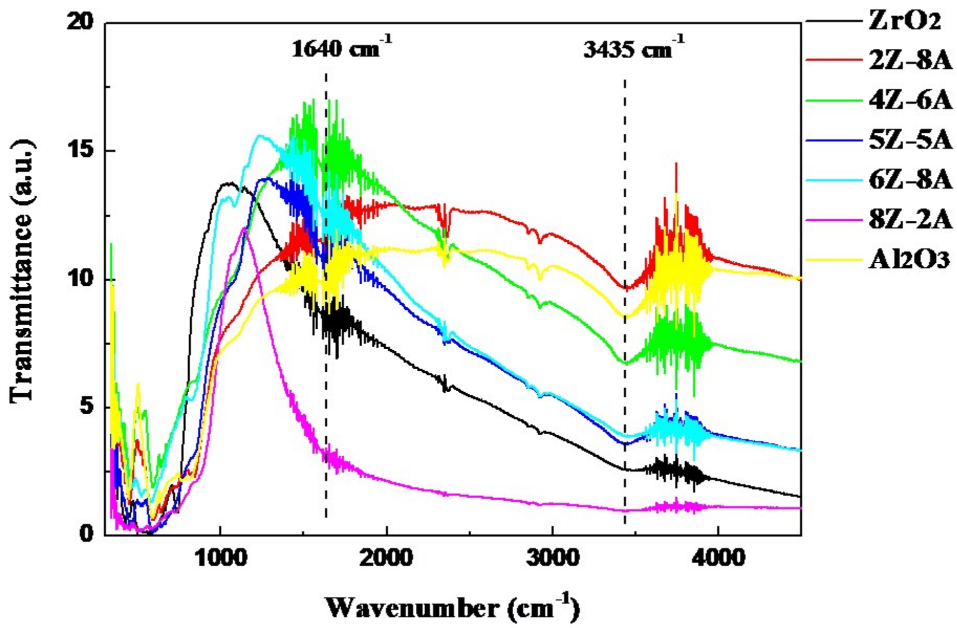

Y. Cong et al. Fig. 7

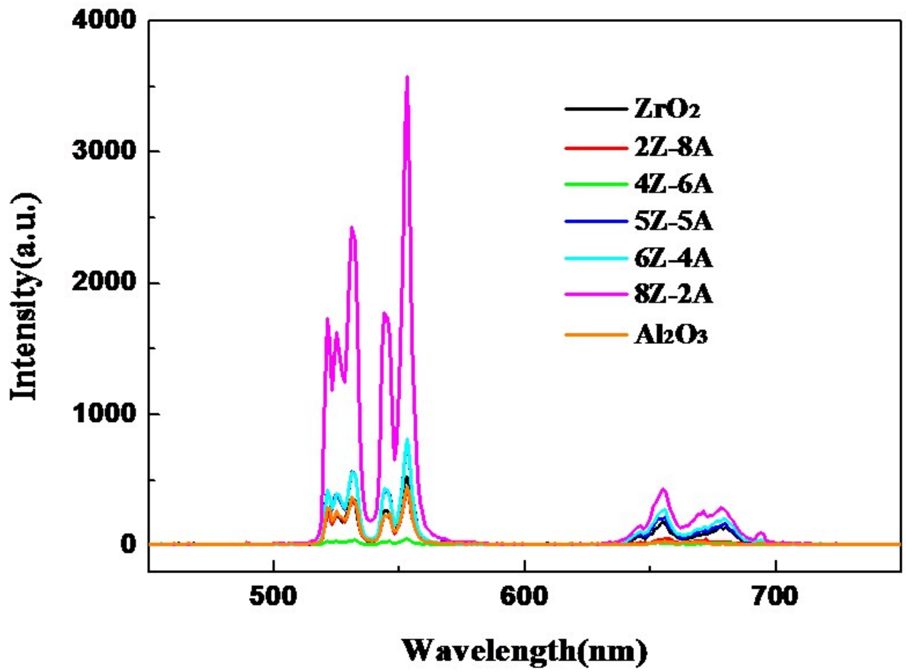

Y. Cong et al. Fig. 8

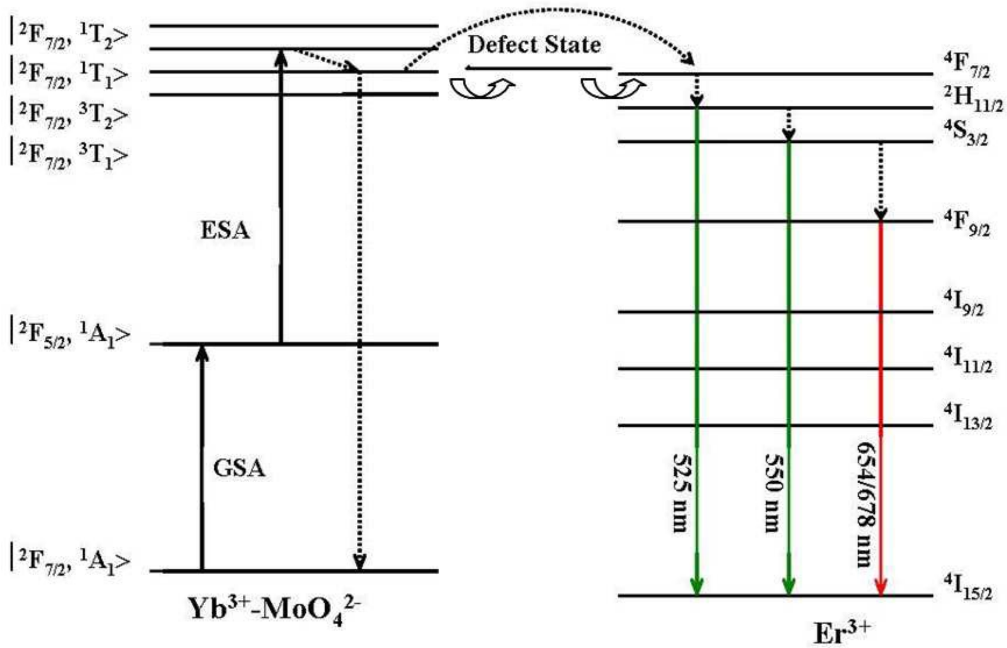

Y. Cong et al. Fig. 9

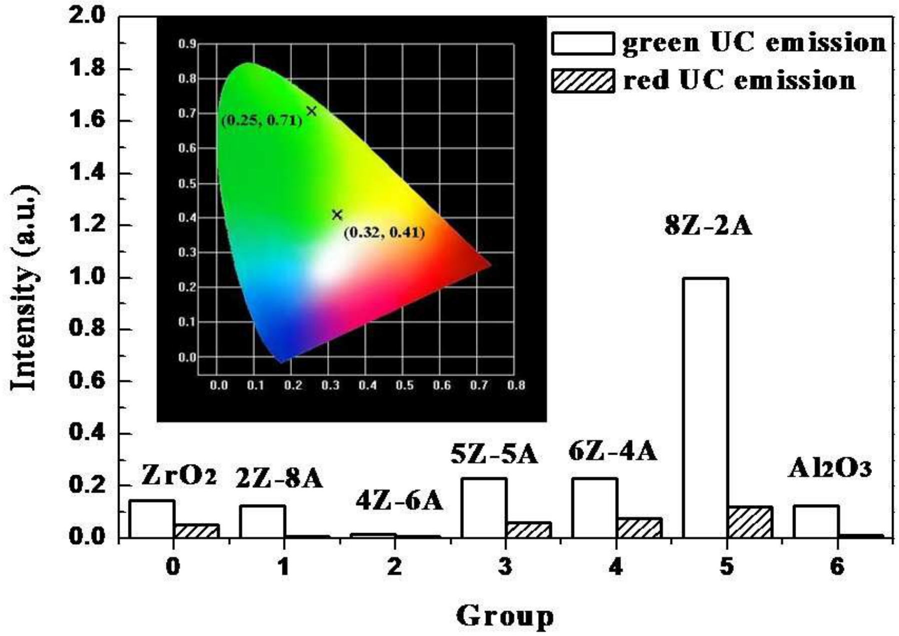

Y. Cong et al. table 1

Samples	8Z-2A	6Z-4A	5Z-5A	4Z-6A	2Z-8A
Er^{3+} content	0.85 mol%	0.24 mol%	0.52 mol%	0.44 mol%	0.26 mol%
	0.1206 wt%	0.0355 wt%	0.0768 wt%	0.0671 wt%	0.0411 wt%